Surface Science 653 (2016) 66–70

Contents lists available at ScienceDirect

Surface Science

journal homepage: www.elsevier.com/locate/susc

Ethylene binding to Au/Cu alloy nanoparticles

Michael D. Gammage [a,*,1], Shannon Stauffer [b,1], Graeme Henkelman [a,b], Michael F. Becker [a,c], John W. Keto [a,d], Desiderio Kovar [a,e]

[a] Materials Science and Engineering Program, The University of Texas at Austin, Austin, TX 78712, United States
[b] Department of Chemistry and the Institute for Computational Engineering and Sciences, The University of Texas at Austin, Austin, TX 78712, United States
[c] Department of Electrical and Computer Engineering, The University of Texas at Austin, Austin, TX 78712, United States
[d] Department of Physics, The University of Texas at Austin, Austin, TX 78712, United States
[e] Department of Mechanical Engineering, The University of Texas at Austin, Austin, TX 78712, United States

ARTICLE INFO

Article history:
Received 22 April 2016
Received in revised form 24 May 2016
Accepted 27 May 2016
Available online 01 June 2016

ABSTRACT

Weak chemisorption of ethylene has been shown to be an important characteristic in the use of metals for the separation of ethylene from ethane. Previously, density functional theory (DFT) has been used to predict the binding energies of various metals and alloys, with Ag having the lowest chemisorption energy amongst the metals and alloys studied. Here Au/Cu alloys are investigated by a combination of DFT calculations and experimental measurements. It is inferred from experiments that the binding energy between a Au/Cu alloy and ethylene is lower than to either of the pure metals, and DFT calculations confirm that this is the case when Au segregates to the particle surface. Implications of this work suggest that it may be possible to further tune the binding energy with ethylene by compositional and morphological control of films produced from Au-surface segregated alloys.

1. Introduction

The massive global production of ethylene and its widespread use in polymer materials warrants investigation of potential efficiency improvements [1]. Fractional distillation is currently widely used for separating ethylene from a cracked gas mixture. This process occurs under high pressure and low temperature, thus making it expensive and energy intensive [2–4]. It has been proposed that selective, permeable membranes could be used to separate ethylene from the cracked gas mixture at a far reduced energy cost [2,3]. Polymer membrane designs have been proposed that utilize Ag(I) and Cu(I) complexation with olefins to enhance separation of gas mixtures; however, the metal ion-olefin complexes are unstable in air, which limits their use in industrial settings [5]. Embedding metallic nanoparticles with a precisely tuned binding energy to ethylene into the polymer membranes would offer improved stability and selectivity of ethylene over ethane compared to aqueous salt-based membranes [6–8]. Previous studies suggest that embedding Ag nanoparticles into a membrane improves selectivity due to the weak chemisorption of ethylene to Ag, although its binding energy is still too strong for viable industrial separations [7]. Alloys may provide a method to tune the binding energy, and thus be an alternative to Ag for ethylene separation. However, for several alloys that were previously investigated [9,10], the binding energies with ethylene were between the pure, end members of the alloys, and therefore were not suitable.

Here, the binding energy of ethylene to Au and Au/Cu alloys are studied. Density functional theory (DFT) is used to calculate the binding energies, of ethylene to Ag, Au, Cu, and Au/Cu alloys and the results suggest that a Au/Cu alloy can have a lower binding energy than either Au or Cu. The binding energies of ethylene to metal surfaces are correlated to the C═C vibrational frequency, ν(CC), which can be measured experimentally. Samples were prepared from the Au and Au/Cu alloys and experimental measurements were made of the surface-enhanced Raman spectra (SERS) at the surfaces of these alloys in the presence of ethylene. The DFT and experimental measurements show good agreement. Subsequent analysis is presented to explain why the binding energy of ethylene to the Au/Cu alloy is weaker than either to pure Au or Cu.

2. Experimental and computational procedures

The laser ablation of microparticle aerosol (LAMA) process was used to produce the metal nanoparticles (NPs) and alloy NPs used in these experiments. LAMA has the advantage that very fast cooling rates allow non-equilibrium alloys to be produced. For example, it has previously been shown that face-centered cubic Au/Cu alloys can be produced with a broad spectrum of compositions, and without bulk phase segregation predicted by the equilibrium phase diagram [11]. Details of the LAMA process are presented elsewhere [12,13], and thus only a summary is presented here.

* Corresponding author.
[1] Both authors contributed equally to this work.

http://dx.doi.org/10.1016/j.susc.2016.05.008
0039-6028/

As shown in Fig. 1a, microparticles of the desired composition (Ag, Au, or Au/Cu alloy particles) were aerosolized using a fluidized bed feeder and the aerosol flowed through an ablation chamber, Fig. 1b. A coaxial buffer gas that surrounded the aerosol was used to constrain the gas through the ablation cell. Helium at 1 atm was used for both the microparticle aerosol and the buffer gas. The microparticle powders used as feedstock for the LAMA process were 1.5–2.0 μm diameter Ag (P-311J, DuPont Inc., Wilmington, DE), 1.5–2.0 μm diameter Au (D100920-68, DuPont Inc., Wilmington, DE), and 44 μm diameter $Au_{0.35}/Cu_{0.65}$ (35Au-65Cu-325MESH, Wesgo Metals, Hayward, CA). A KrF excimer laser (Lumonics Pulsemaster PM-848, Nepean, ON, Canada) with a pulse energy of 250 mJ, wavelength of 248 nm, and pulse-width of 12 ns was focused onto the aerosol to an area of 3 mm × 1.5 mm using cylindrical lenses, which resulted in a fluence on the microparticles of ~2.8 J/cm^2. Previous research has shown that the size distributions for metal NPs are bimodal with a width (standard deviation) from both modes that is 35% of the mean [14]. In a different study, Au/Cu NPs were shown to have a mean diameter of 8.5 ± 3.5 nm when ablated in a N_2 aerosol at 1 atm [11]; the mean diameter decreased by 38% for NPs ablated in He aerosols, such as the samples produced for this study [14].

A supersonic deposition process was used to impact the LAMA-produced NPs to produce films with nanoscale roughness [15]. The NP aerosol was first routed through a virtual impactor, shown schematically in Fig. 1c, to separate any unablated particles. The aerosol was then directed to a flat-plate nozzle with a diameter and plate-thickness of 250 μm. The substrates were placed on an x-y motorized stage inside the deposition chamber, which was pumped down to <27 Pa using a mechanical vacuum pump backing a root blower that had a combined capacity of 5500 l/min. The pressure differential at the nozzle accelerated the NPs to a velocity of ~600 m/s prior to impaction onto aluminum substrates [15]. The substrates were translated, as shown in Fig. 1d, using x-y stepper motors to pattern a film with x-y-z dimensions of 3 mm × 3 mm × ~100 μm.

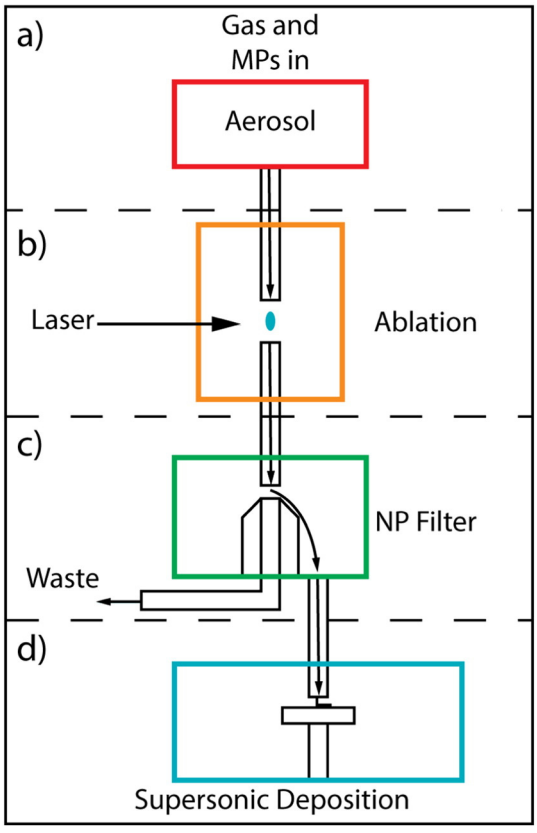

Fig. 1. Schematic of the laser ablation of microparticle aerosol (LAMA) process showing (a) aerosol generation, (b) ablation cell, (c) virtual impactor, and (d) supersonic impaction deposition chamber.

The resulting films were used as SERS substrates in a custom-built gas chamber to measure the Raman spectra of ethylene gas on the metal NPs. A Raman microscope (Horiba LabRam HR, Kyoto, Japan) was used with a 633 nm laser at ~2 mW laser power and a 20× super long working distance objective for the Au and Au/Cu samples. Another Raman microscope (WiTec Alpha300 R, Ulm, Germany) with a 488 nm laser at 2–10 mW and a 20× long working distance objective (Zeiss LD Plan-Neofluar 20x/0.4 Corr Ph2) was used for the Ag samples. For both instruments, the custom gas chamber was filled with 2 atm of 99.999% ethylene and Raman spectra were measured from the surfaces of the films. The peak locations in these spectra were related to the binding energies using the calculated correlations between the C═C vibrational frequency and the binding energies (discussed in more detail in the section that follows). For comparison with the LAMA-produced films, commercially available SERS substrates of Ag and Au were also obtained and tested (SERStrates, Silmeco, Copenhagen, Denmark).

For modeling, the energies were calculated with DFT as implemented in the Vienna ab initio simulation package [16]. The projector-augmented wave framework was used to describe the core electrons [17,18] and valence electrons were described by single-electron Kohn-Sham wave functions [19,20]. The generalized gradient approximation with the PBE functional was used to describe electronic correlation and exchange. The wave functions of the valence electrons were expanded in a plane-wave basis set up to a kinetic energy cutoff of 300 eV; increasing this cutoff to 350 resulting in changes of binding energy of only 0.005 eV. Spin-polarization was considered in all cases. Gaussian-type smearing with a width of 0.01 eV around the Fermi level was used to improve convergence. All systems were optimized to their ground-state geometry until the forces on each atom were less than 0.01 eV/Å.

Two geometries were considered, metallic NPs and slabs. Metallic NPs were modeled with 79-atom in a face-centered cubic (FCC) lattice and a truncated octahedral geometry with 8 Å of vacuum separating periodic images. Slabs were constructed with the lowest energy {111} surface planes. Four layers were used to describe all slabs except the alloy for which five were used. Lattice constants were determined from relaxation of bulk cells; the bottom two layers of the slabs were frozen in these bulk geometries. The slabs were separated by 20 Å of vacuum. The Brillouin zone was sampled at the Γ-point for the NPs and a 4 × 4 × 1 k-point mesh for the slabs. In the alloys, atoms were randomly assigned element types consistent with the overall composition.

Vibrational frequencies were calculated by diagonalization of the Hessian matrix, constructed by displacement of all atoms in the ethylene molecule by a finite-difference step size of 0.01 Å. Dispersion corrections were tested using the Tkatchenko-Scheffler method [21, 22] and were found to increase binding energies by ~0.3 eV and decrease phonon frequencies by no more than 15 cm^{-1}. The trends in binding energy and frequencies were not significantly impacted, thus dispersion corrections were not applied to the reported values. It is well documented that DFT calculations using generalized gradient-approximation (GGA) functionals tend to underestimate lattice constants and thus also underestimate vibrational mode frequencies [23].

3. Results

Experimental Raman spectra for ethylene on $Au_{0.35}/Cu_{0.65}$, Au, and Ag are shown in Fig. 2. Broad peaks are clearly observed that correspond to the ν(CC) mode, and the centroids of those peaks are at ~1590 cm^{-1} for Ag and $Au_{0.35}/Cu_{0.65}$ and at ~1560 cm^{-1} for Au. In addition, the δ(CH_2) mode is observed at ~1325 cm^{-1} for $Au_{0.35}/Cu_{0.65}$ and Au and at ~1350 cm^{-1} for Ag. In previous studies, it was shown that the ν(CC) mode for ethylene was at 1539 cm^{-1} on Au films and 1543 cm^{-1} on Cu films [25]. What is remarkable about the data in

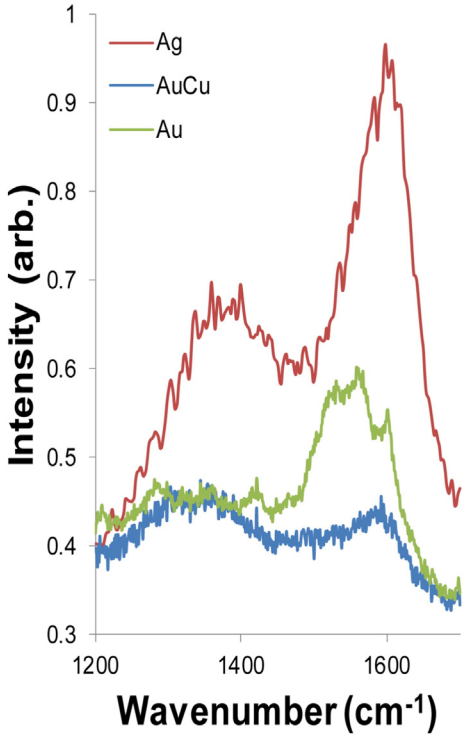

Fig. 2. Raman spectrum for ethylene on a SERS $Au_{.35}/Cu_{.65}$ alloy (blue) film. The C═C peak of ethylene is shifted from the unbound position of 1623 cm^{-1} [24] to ~1590 cm^{-1}. The spectra for ethylene on SERS Ag (red) and Au (green) NP films are also shown for reference. (For interpretation of the references to color in this figure legend, the reader is referred to the web version of this article.)

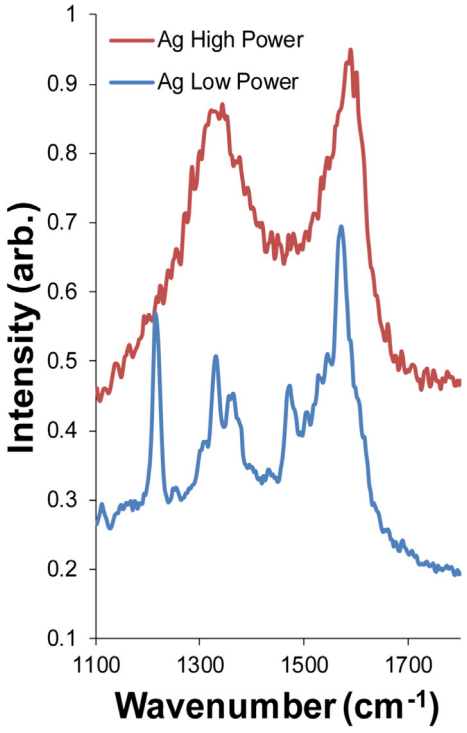

Fig. 3. Raman spectra measured at two laser intensities for ethylene on commercially obtained Ag SERS substrates near the frequency of the C═C stretch. The peak breadth increases with laser power. The spectral intensities were scaled for ease of viewing.

Fig. 2 is that the ν(CC) mode of ethylene on the Au/Cu alloy is higher than either Au or Cu, indicating that the binding energy for the alloy is lower than for either Au or Cu.

The breadth of the peaks in the Raman spectra shown in Fig. 2 was considerably broader than those measured previously [25]. It should be noted that the current measurements were made using ethylene gas whereas the previous measurements were made after condensing the ethylene onto the SERS films. Measurements made on commercial Ag SERS substrates (see Fig. 3) using ethylene gas also show considerably sharper peaks than those obtained on LAMA-produced films, indicating that some of the source of the broadening is related to characteristics of the LAMA film. However, the peak widths measured from commercial SERS substrates are still considerably broader than those obtained previously on metal films using condensed ethylene. As shown in Fig. 3, increasing the laser power from ~0.1 mW to ~0.5 mW (corresponding to fluences of ~880 and ~4400 W/cm^2, respectively) further broadened the peaks. Observations of the surfaces of the LAMA-produced films in a scanning electron microscope revealed that, although they were relatively rough at the nanoscale, regularly spaced gaps between the NPs were largely absent. It is well known that the gap spacing plays a critical role in peak enhancement in SERS [26], so non-optomized gap sizes such as observed in the LAMA-produced films would be expected to significantly weaken and broaden the SERS spectra. Further weakening and broadening are expected in Au and Au/Cu alloys relative to Ag since previously it has been shown that peak intensities decrease going from Ag to Cu to Au [25]. For the current experiments, the advantages of LAMA in being able to produce quantities of non-quilibrium alloy NPs sufficient to produce thick films, outweighs their non-optomized performance as SERS substrates compared to commerical substrates.

DFT calculations of ethylene binding to pure Au, Cu, Ag and alloy Au/Cu systems were conducted in an effort to explain the observed Au/Cu alloy Raman spectra. Small, ~1.0 nm (79-atom) NPs and infinite slab surfaces were considered, and it was found that size effects did not significantly affect the trends in binding energies and frequencies across compositions that are of most interest here. Different binding sites exhibited similar trends for 79-atom NPs and slabs, which is consistent with previous findings [7]. NPs with 79-atoms were therefore initially sampled for trends in binding energy over a range of binding sites and NP compositions. Fig. 4 shows the predicted binding energy versus C═C stretch frequency for different binding sites of Ag, Au, Cu, and Au/Cu alloy 79-atom NPs. A nearly linear correlation is apparent between the binding energy and the frequency with Ag{111} face sites having the weakest binding (highest ν(CC) frequency), followed by the Ag edge (step), Au{111} face and the Cu edge sites. Cu{111} face sites are an outlier having similar binding energy to Au{111} sites, but much lower frequency than Ag edge (step) sites. These results are consistent with the predictions of a previous study that showed that ethylene binds strongly to edge sites and less strongly to {111} surfaces for all systems [7]. This linear correlation of C═C stretch frequency and ethylene binding energy holds for Au/Cu random alloy particles as well, with the binding energies and ν(CC) frequencies lying within the range of the pure Au and Cu systems.

In our search for a plausible theoretical model for the measured ethylene on Au/Cu alloy Raman spectra, we identified a trend in binding energy for both pure metal NPs and alloyed Au/Cu NPs, but the predicted range of binding energies and frequencies of the $Au_{0.35}/Cu_{0.65}$ random alloy NPs using this approach is between its end-member metal NPs, Au and Cu, which is not consistent with the experimentally determined Raman spectra. To understand the source of this inconsistency, it was necessary to consider likely scenarios for preferential ethylene binding and surface segregation. Ethylene binding to Cu sites on an alloy surface is stronger than binding to Au sites of equivalent alloys, and thus ethylene should preferentially bind to all available Cu sites before Au. For a $Au_{0.35}/Cu_{0.65}$ random alloy, a majority of surface sites would be Cu, and since ethylene strongly binds to Cu, the average ν(CC) stretching frequency would be lower than for ethylene adsorbed on a Au surface.

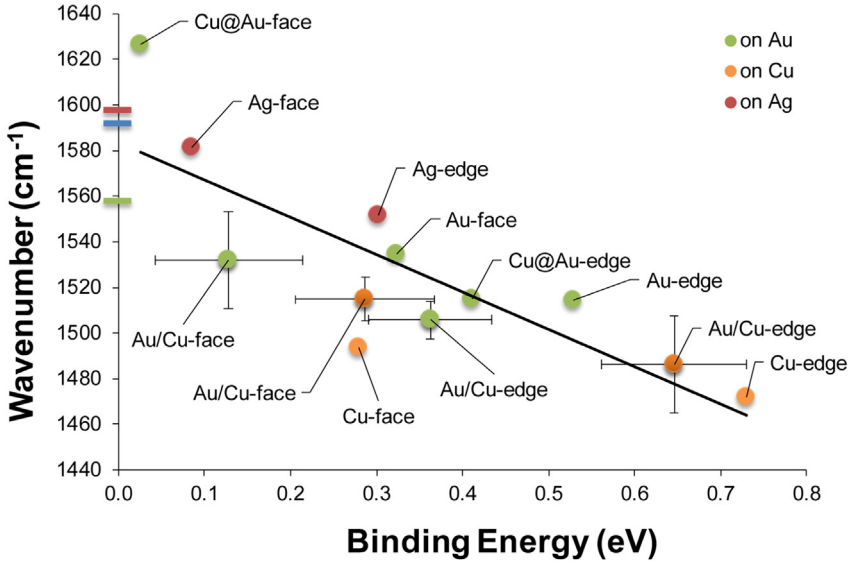

Fig. 4. Calculated binding energy versus C═C stretch frequency for 79 atom Ag, Au, Cu, $Au_{0.35}Cu_{0.65}$ and Cu@Au (coreshell) NPs on different binding sites. Random $Au_{0.35}/Cu_{0.65}$ alloys (labeled Au/Cu) are shown with the standard deviation of 30 samples, and single calculations were carried out for all other NPs, since there is only one composition possible with these models. Data are presented by the adsorbing metal, Ag (red), Au (green) and Cu (orange) and are given as e.g. Ag-face (model composition-binding site). Experimental frequencies are indicated on the y-axis, Ag (red), Au/Cu (blue), Au (green). (For interpretation of the references to color in this figure legend, the reader is referred to the web version of this article.)

The SERS Au/Cu film, though, had a measured ν(CC) frequency much higher than that of the SERS Au film, 1590 and 1560 cm^{-1}, respectively. This suggests that the ethylene binding measured is ethylene bound to Au sites. These results can be explained by preferential segregation of Au atoms to the surfaces of the Au/Cu alloys, and indeed this is the expected behavior in the Au/Cu system [27]. To test whether segregation of Au to the surface is thermodynamically stable, we swapped the identity of a surface Cu to Au for a $Au_{0.35}/Cu_{0.65}$ random alloy NP. The energy difference of the swapped NP and the original configuration was −0.21 eV, indicating that it is thermodynamically favorable for Au to segregate to the surface. X-ray photon spectroscopy (XPS) performed on our Au/Cu film was consistent with this hypothesis. XPS conducted on the surface of the Au/Cu film showed the presence of only Au but sputtering to remove the surface revealed the presence of both Au and Cu.

Accordingly, we considered a model in which Au was segregated to the surface of the Au/Cu alloy particle. This model was the core@shell Cu@Au 79-atom NP shown in Fig. 5a. The binding energy of ethylene on a {111} facet is appreciably weaker for the alloy, 0.03 eV, than a pure Au or Ag metal NP, 0.32 and 0.09 eV, respectively, while binding to an edge site, 0.41 eV, is within the range for random alloy NP binding sites. The predicted C═C stretch frequency for ethylene bound to a Cu@Au NP on the {111} facet and edge site are 1674 cm^{-1} and 1563 cm^{-1}, respectively.

Since the nanoparticles in the SERS film were larger than our model, and actually in the range of 2–8 nm, we repeated our calculations for the large-size limit: metal slabs. Specifically, we choose the lowest energy {111} surface, which is expected to dominate in the experiment. Fig. 6 shows the results for Ag, Au, and Cu slabs compared to a $Au_{0.35}/Cu_{0.65}$ random alloy slab with a monolayer of gold on the surface (denoted as AuCu@Au) shown in Fig. 5b. The results are consistent with the NP calculations. The AuCu@Au slabs were found to weakly adsorb ethylene to the surface with a ν(CC) stretching frequency of ~30 cm^{-1} higher than an Ag{111} surface; a shift of 70 cm^{-1} was calculated for the Cu@Au.

4. Discussion

In a previous theoretical report, adsorption energy to a core@shell NP was at the extremes of the alloy end-members [28], and a related

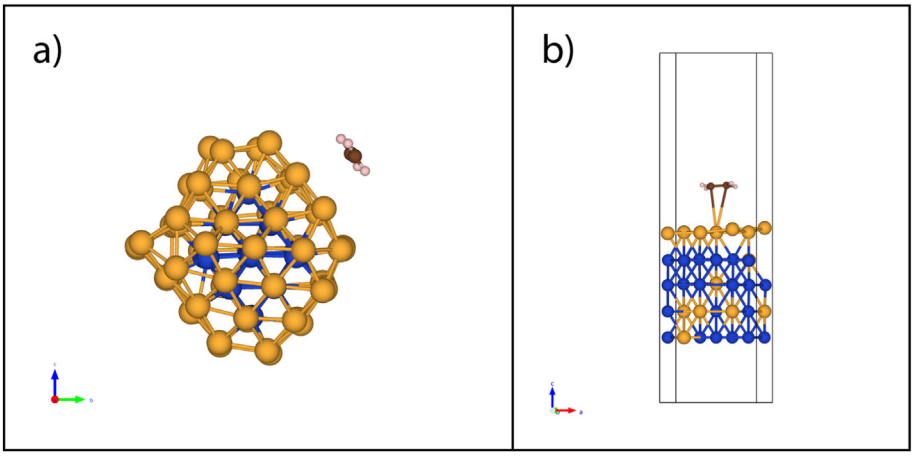

Fig. 5. Image of a) the Cu@Au79-atom NP with adsorbed ethylene on a {111} facet site—Cu atoms (blue), Au (yellow), C (brown) and b) AuCu@Au with an adsorbed ethylene molecule—Cu atoms (blue), Au (yellow), and C (brown). (For interpretation of the references to color in this figure legend, the reader is referred to the web version of this article.)

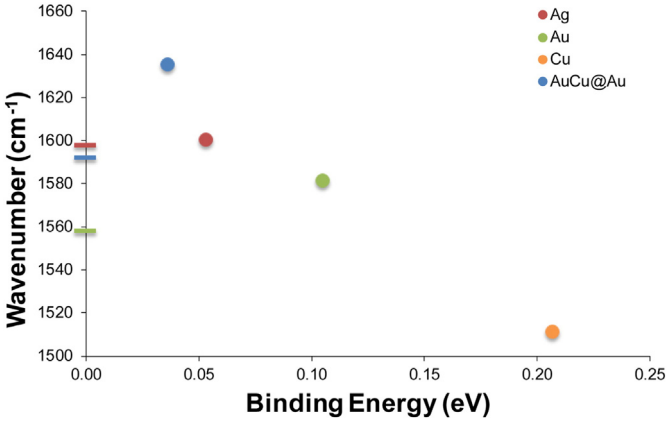

Fig. 6. Binding energy versus C═C stretch frequency of ethylene on $Au_{0.35}/Cu_{0.65}$ random alloy slab with a surface layer of gold (denoted as AuCu@Au). The calculated value for Ag, Au, and Cu slabs are given for reference, as well as the experimental values on the y-axis, Ag (red), Au/Cu (blue), Au (green). (For interpretation of the references to color in this figure legend, the reader is referred to the web version of this article.)

experimental report noted the segregation of a more noble metal to the surface of a NP increased the catalytic activity of the substrate [29]. In the Au/Cu alloy system studied here, we found that the binding energy of ethylene to the Cu@Au{111} facets is lower than either end-member. Experimental and theoretical evidence suggest that the nanoparticle film is Au-surface enriched. The calculated weaker binding energy on this surface corresponds to a higher ν(CC) frequency than on Ag by 30 cm^{-1}, pushing the predicted frequency above the measured Au/Cu SERS peak. The Au-surface segregated model therefore provides a plausible explanation for the experimental frequency shifts measured in SERS experiments of Au/Cu films.

5. Conclusions

Since weak chemisorption of ethylene is crucial to developing a facilitated transport, nanoparticle composite membrane, a promising Au/Cu alloy was studied using a combination of DFT modeling and SERS measurements. It was found that ethylene has a similar binding energy to $Au_{0.35}/Cu_{0.65}$ and Ag surfaces, and a considerably lower binding energy than to Au or Cu and this was rationalized by showing that Au segregates to the surface of $Au_{0.35}/Cu_{0.65}$ alloys. An optimal alloy for a nanoparticulate membrane for separations should have an even lower binding energy to ethylene than that measured here for Ag and the $Au_{0.35}/Cu_{0.65}$ systems [6]. The current work suggests that, this may be possible via a thorough screening of compositions and surface structures of Au/Cu alloy nanoparticles.

Acknowledgements

We gratefully acknowledge the support from the National Science Foundation (CBET 0708779 and CMMI 1435949), the Welch Foundation (grant F-1841) and the Texas Advanced Computing Center. We would also like to thank Dr. Richard Piner for his assistance with the Raman experiments.

References

[1] R. Baum, Chemical & Engineering News 86 (2008) 35.
[2] T. Ren, M.K. Patel, K. Blok, Energy 33 (2008) 817.
[3] R.B. Eldridge, Ind. Eng. Chem. Res. 32 (1993) 2208.
[4] F.B. Petlyuk, Distillation Theory and Its Application to Optimal Design of Separation Units, Cambridge University Press, Cambridge, UK, 2004.
[5] H.S. Kim, J.H. Ryu, H. Kim, B.S. Ahn, Y.S. Kang, Chem. Commun. 14 (2000) 1261.
[6] Z.D. Pozun, G. Henkelman, J. Membr. Sci. 364 (2010) 9.
[7] Z.D. Pozun, K. Tran, A. Shi, R.H. Smith, G. Henkelman, J. Phys. Chem. C 115 (2011) 1811.
[8] D.F. Sanders, Z.P. Smith, R. Guo, L.M. Robeson, J.E. McGrath, D.R. Paul, B.D. Freeman, Polymer 54 (18) (2013) 4729.
[9] P.A. Sheth, M. Neurock, M.C. Smith, J. Phys. Chem. B 109 (25) (2005) 12449.
[10] D. Mei, M. Neurock, Topics in Catalysis 20 (1) (2002) 5.
[11] Malyavanatham, G., O'Brien, D. T., Becker, M. F., Keto, J. W., and Kovar, D., Au/Cu nanoparticles produced by laser ablation of mixtures of Au and Cu microparticles. J. Nanoparticle Res. 2004, 6[6] 661–64.
[12] M.F. Becker, J.R. Brock, H. Cai, D. Henneke, L. Hilsz, J.W. Keto, J. Lee, W.T. Nichols, H.D. Glicksman, Nanostruct. Mater. 10 (1998) 853.
[13] W. Nichols, J.W. Keto, D.E. Henneke, J.R. Brock, G. Malyavanatham, M.F. Becker, H.D. Glicksman, Appl. Phys. Lett. 78 (2001) 11281130.
[14] W.T. Nichols, G. Malyavanatham, D.E. Henneke, J.R. Brock, M.F. Becker, J.W. Keto, H.D. Glicksman, J. Nanopart. Res. 2 (2) (2000) 141.
[15] C. Huang, W. Nichols, D.T. O'Brien, M.F. Becker, D. Kovar, J.W. Keto, J. Appl. Phys. 101 (6) (2007) 064902.
[16] G. Kresse, J. Hafner, Phys. Rev. B 47 (1993) R558.
[17] P. Hohenberg, W. Kohn, Phys. Rev. 136 (1964) 864.
[18] W. Kohn, L.J. Sham, Phys. Rev. 140 (1965) 1133.
[19] P.E. Blöchl, Phys. Rev. B 50 (1994) 17953.
[20] G. Kresse, D. Joubert, Phys. Rev. B 59 (1999) 1758.
[21] J.P. Perdew, Y. Wang, Phys. Rev. B 45 (1992) 13244.
[22] A. Tkatchenko, M. Scheffler, Phys. Rev. Lett. 102 (2009) 073005.
[23] J.P. Perdew, A. Ruzsinszky, G.I. Csonka, O.A. Vydrov, G.E. Scuseria, L.A. Constantin, X. Zhou, K. Burke, Phys. Rev. Lett. 100 (2008) 136406.
[24] T. Shimanouchi, J. Phys. Chem. Ref. Datas 6 (3) (1977) 993.
[25] W. Akemann, A. Otto, Langmuir 11 (4) (1995) 1196.
[26] Xie, W. and Schlücker, S., Rationally designed multifunctional plasmonic nanostructures for surface-enhanced raman spectroscopy: a review. Reports on progress in physics, Physical Society 2014 (Great Britain), 77.11, 116502.
[27] G. Guisbiers, R. Mendoza-Cruz, L. Bazán-Díaz, J.J. Velázquez-Salazar, R. Mendoza-Perez, R.-L. Robledo-Torres, J.L., J.M. Montejano-Carirzales, R.L. Whetten, M. José-Yacamán, ACS Nano 10 (2015) 188.
[28] W. Tang, L. Zhang, G. Henkelman, J. Phys. Chem. Lett. 2 (2011) 1328.
[29] S. Koh, P. Strasser, J. Am. Chem. Soc. 129 (2007) 12624.